Global Journal of Researches in Engineering: F
Electrical and Electronics Engineering
Volume 21 Issue 3 Version 1.0 Year 2021
Type: Double Blind Peer Reviewed International Research Journal
Publisher: Global Journals
Online ISSN: 2249-4596 & Print ISSN: 0975-5861

A High-Precision Low-Cost Analog Acceleration and Vibration Amplifier using PVDF Piezoelectric Sensors

By Thomas L. Hemminger

Abstract- This paper describes a high-resolution analog acceleration and vibration amplifier for use with piezoelectric polyvinylidene fluoride (PVDF) sensors. The purpose of this system is to monitor automated parts placement on integrated circuit boards. One of the problems facing production and inspection equipment is the occurrence of resonant and ambient vibrations. Even small errors can cause systems with micrometer and nanometer precision to exceed design tolerances. This work describes a method to monitor mechanical vibrations through a portable and inexpensive signal-processing unit. The system provides user-selectable gain and filtering modules that are compact and reliable. PVDF is currently used in sensing applications, and its material properties have proven very useful for sensing mechanical stress, strain, pressure, and temperature.

Index Terms: *PVDF, piezoelectric film, vibration sensing, Sallen-Key.*

GJRE-F Classification: *FOR Code: 290901*

Strictly as per the compliance and regulations of:

A High-Precision Low-Cost Analog Acceleration and Vibration Amplifier using PVDF Piezoelectric Sensors

Thomas L. Hemminger

Abstract- This paper describes a high-resolution analog acceleration and vibration amplifier for use with piezoelectric polyvinylidene fluoride (PVDF) sensors. The purpose of this system is to monitor automated parts placement on integrated circuit boards. One of the problems facing production and inspection equipment is the occurrence of resonant and ambient vibrations. Even small errors can cause systems with micrometer and nanometer precision to exceed design tolerances. This work describes a method to monitor mechanical vibrations through a portable and inexpensive signal-processing unit. The system provides user-selectable gain and filtering modules that are compact and reliable. PVDF is currently used in sensing applications, and its material properties have proven very useful for sensing mechanical stress, strain, pressure, and temperature.

Index Terms: PVDF, piezoelectric film, vibration sensing, Sallen-Key.

I. Introduction

As the integration level of electronic systems increases and becomes more sophisticated, producing these devices grows more complicated and expensive. Not only does fabrication become increasingly difficult, but inspection and testing are also more demanding. One of the problems facing automated production and inspection equipment is resonant and ambient vibration. The design described here was motivated by the specific needs of an industrial sponsor. However, it can be useful for many applications requiring low-cost sensors for monitoring vibrations and accelerations. Polyvinylidene Fluoride (PVDF) is an extremely effective material for converting mechanical movements into electrical signals and has some of the strongest piezoelectric effects of all known polymers [1]. This property makes the material an effective candidate for use in the construction of vibration and acceleration sensors [2]-[7]. There are, however, some disadvantages when working with PVDF. Not only does it exhibit a high piezoelectric constant, but also a considerable pyroelectric constant, indicating that the material produces high voltage variations when exposed to changes in temperature. There can be as much as an 8-volt change in output voltage per degree Celsius [8]. This can be managed with a combination of shielding and a DC offset control. PVDF material is also highly capacitive and is sensitive to IR and RF interference, but careful design can reduce these effects. All of these potential problems were considered and addressed in the finished system.

Initially, several currently available designs were evaluated to investigate the properties of PVDF sensors and the signal processing characteristics of the associated amplifiers [9]. Improved amplification and conditioning circuitry was designed, constructed, and tested for use with several types of these sensors. Frequency response, dynamic range, and measurement axes are important, but cost is another important factor. The analog system described here is robust, low-cost, and portable. It can employ batteries, a single +5volt supply, or a plug-in wall adapter. Excessive vibrations are indicated through a simple LED arrangement, or the system can be connected to a data acquisition recorder for time and/or frequency analysis. The specifications for the overall system are illustrated in Table 1.

Table 1: Required signal conditioner specifications

Parameter	Specification
Frequency Range	0 Hz to 10 kHz, at selectable ranges
Filter roll-off	60 dB/decade
THD	<0.02%
Linearity	<0.2% deviation
Resolution	$0.1\mu g/\sqrt{Hz}$ in conjunction with sensor
Gain	Selectable up to 150
Thermal Stability	Minimal effect
Dynamic Range	$\pm 50\,g$
Transverse Sensitivity	< 1%
Output	+/- 10V

II. System Design

This design is composed of seven blocks, which are described in the following subsections. The high-pass and low-pass filters are of similar configuration. Therefore, only the high-pass filters will be described in detail. Component values are included for all of the filtering elements. A block diagram of the conditioner is shown in Fig. 1.

Author: Ph.D, School of Engineering, Penn State Erie, The Behrend College, Erie, PA 16563. e-mail: tlh5@psu.edu

a) Power supply

One specification required of this design is that it operates from a single 5-volt DC power supply. Therefore, a Newport NMA0512S one-watt to DC-to-DC converter was employed to power all components. This model has an internal oscillation frequency of 100 kHz, which is well beyond the frequency ranges being monitored. The low-power design presented here lends itself to battery operation, which is advantageous over plug-in wall adapters because of AC line interference.

b) Input impedance control

High input impedance is necessary to successfully measure PVDF sensor signals at low frequencies. This is due to the capacitance characteristics of the film [10-11]. The capacitance of PVDF is a function of its geometry, indicating that the cutoff frequency is usually determined by the amplifier input impedance alone ($f_e = 1/2\pi RC$). For example, if an amplifier has an input impedance of $10k\Omega$ for a given PVDF capacitance of *3nF* it yields a cutoff frequency of 5.3*kHz* which is unacceptable for this application. One goal is to amplify signals of very low frequency near the DC level. To achieve lower cutoff frequencies the input resistance of the amplifier must be increased. Consequently, a non-inverting JFET voltage follower with an input impedance of about $10^{12}\Omega$ was chosen to enable measurements at very low frequencies. This produces a cutoff frequency of about $5.3x10^{-5}Hz$. The drawback to a non-inverting buffer is that input bias currents of the op-amp cause the amplifier to saturate. This condition can be alleviated by providing another high impedance path to ground (see Fig. 2). The value of *R* must be high enough to provide a cutoff frequency below the lowest frequency of interest. For example, to achieve a cutoff frequency of 10 Hz with a sensor that has a capacitance of *3nF* would require a $5.3M\Omega$ resistor. For this example, $R = 50\ M\Omega$ which results in a cutoff frequency of about 1 Hz which fits the required specifications. The impedance control resistor determines the input impedance of the buffer so this resistance should be chosen with knowledge of the physical characteristics of the sensors to be used with the system.

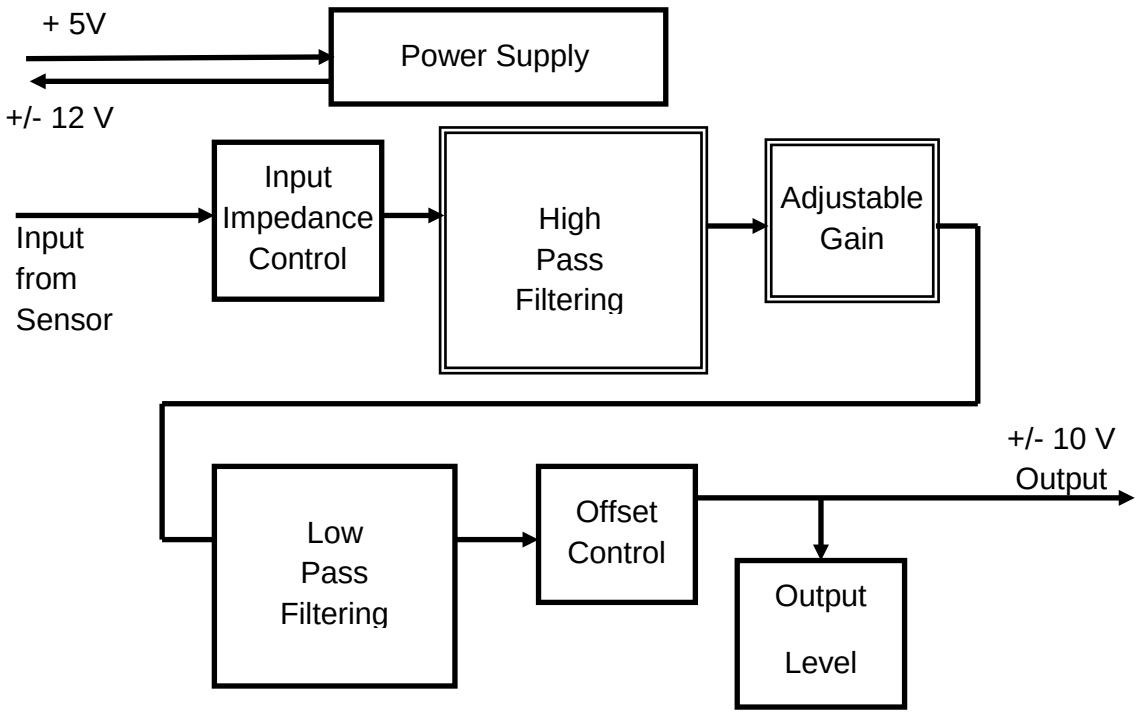

Fig. 1: High-level design of the signal conditioner

Because of the possibility of high voltage spikes from PVDF sensors, the design includes two zener diodes to regulate the input signal. Diodes should be chosen with breakdown voltages higher than the op-amp supply voltage. For the prototype amplifier, zener diodes with a 20V breakdown voltage were selected.

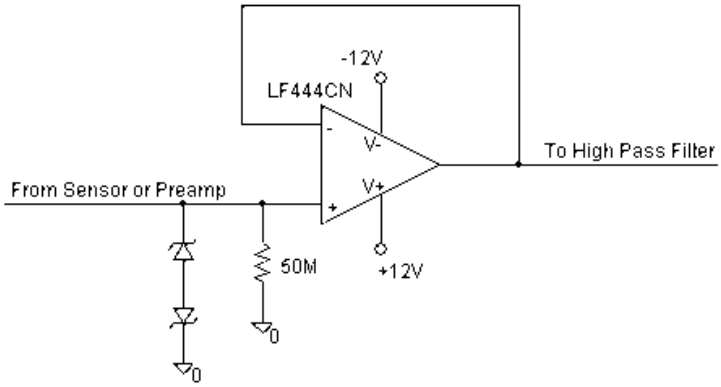

Fig. 2: Input buffer and impedance control circuit with over-voltage protection

c) Filter Banks

G-force amplitudes and corrupting frequencies have been a concern. Therefore it was decided to have a selectable frequency range via switches on the circuit board. A range of high-pass and low-pass filters in a cascade arrangement was decided upon, each having the ability to be independently activated. The low-pass cutoff frequencies were 100 Hz, 500 Hz, 1 kHz, and 10 kHz. The high-pass cutoffs were 3Hz, 100 Hz, 500 Hz, and 1 kHz. With this design the user may select 15 combinations of high-pass and low-pass filters. An "all-pass" switch has been included in both filter banks as a bypass. The LF347 op-amp was chosen because it has several useful features, e.g., extremely high input impedance (10^{12} Ω), low input bias current (50 pA), and wide bandwidth (4 MHz).

Several active filter models were investigated, but after reviewing the tradeoffs, the Sallen-Key configuration was most suitable [12-14]. The high-frequency specification for this system is 10 kHz, which is well below the 1 MHz level at which this filter begins to degrade. Also, since the amplification is done in a separate circuit, all filter stages are unity gain, alleviating gain-bandwidth product issues. Filter selectivity is certainly an important factor but linear phase response is also significant, so only two filter families were explored i.e., Butterworth and Bessel. The Butterworth has a much stronger roll-off than the Bessel, but the phase response is not as flat. However, Bessel filters have such a gradual roll-off that the required order becomes prohibitive. Also, as shown in Fig. 3, the phase response of the Butterworth is nearly linear in the pass-band, translating into an acceptable group delay. Further examination of the delay shows us that it has little effect on the output of the filters. The delay is uniform through the majority of the pass-band—up approximately 4 kHz for 4th order. This was verified by comparing the total harmonic distortion of these two filters at frequencies near the cutoff. For 5 kHz, 9 kHz, and 10 kHz input signals the THD of both filter types is less than 0.006%. For these reasons the Butterworth was chosen.

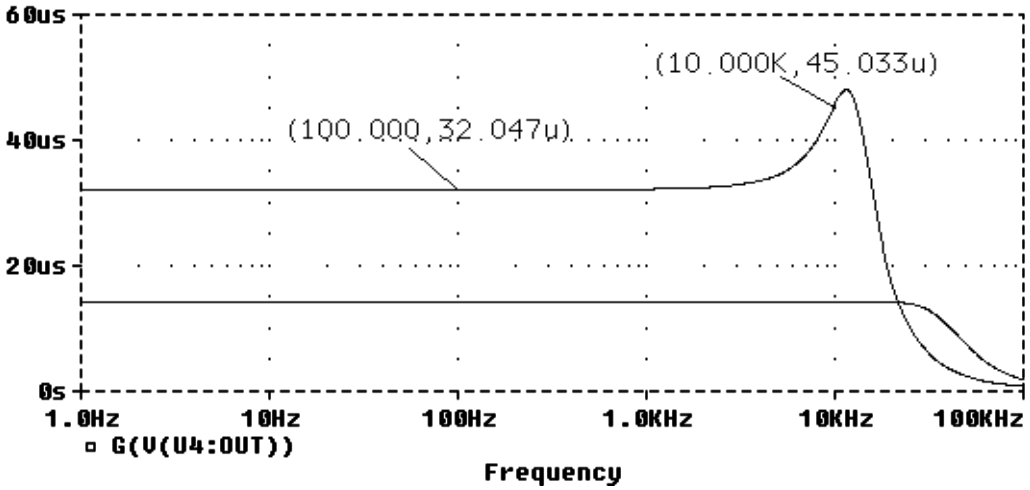

Fig. 3: Butterworth filter versus Bessel filter group delay comparison

Eight filters were designed for this research project. One tool employed was the Filter Pro low-pass filter design program from Texas Instruments. A MATLAB program was also written to verify the results of Filter Pro, and to aid in the selection of component values. The transfer functions for the 2nd order low-pass and high-pass Sallen-Key are shown here:

$$H(s) = \frac{K\dfrac{1}{C_1C_2R_1R_2}}{s^2 + s\left[\dfrac{1}{C_2R_2} + \dfrac{1}{C_2R_1} + \dfrac{1-K}{C_1R_1}\right] + \dfrac{1}{C_1C_2R_1R_2}} \quad (1)$$

$$H(s) = \frac{K}{1 + \dfrac{R_2(C_1+C_2) + R_1C_2(1-K)}{\varpi_c R_1R_2C_1C_2}\cdot\dfrac{1}{s} + \dfrac{1}{\varpi_c^2 C_1C_2R_1R_2}\cdot\dfrac{1}{s^2}} \quad (2)$$

Each filter used in this project comprises two cascaded 2-pole filters, yielding a 4-pole configuration with all filters designed to have less than 0.5 dB attenuation in the pass-band. Fig. 4 illustrates the layouts of the high-pass and low-pass 4-pole Sallen-Key filters. Values for all resistive and capacitive components are shown in table 2.

Table 2: Low-pass and high-pass filter component values

	Freq.	R1	R2	R3	R4	C1	C2	C3	C4
Low-Pass	100 Hz	2.32 kΩ	21.2 kΩ	18.2 kΩ	18.9 kΩ	1.0 nF	3.3 nF	470 pF	10 nF
	500 Hz	1.66 kΩ	16.3 kΩ	2.33 kΩ	19.0 kΩ	6.8 nF	22 nF	3.3 nF	22 nF
	1 kHz	2.18 kΩ	18.4 kΩ	1.59 kΩ	17.2 kΩ	22 nF	68 nF	10 nF	220 nF
	10 kHz	8.93 kΩ	37.5 kΩ	3.55 kΩ	18.9 kΩ	20 nF	220 nF	100 nF	220 nF
High-Pass	3 Hz	17.6 kΩ	15.0 kΩ	42.4 kΩ	6.21 kΩ	3.3 µF	3.3 µF	3.3 µF	3.3 µF
	100 Hz	15.5 kΩ	11.3 kΩ	26.6 kΩ	3.89 kΩ	220 nF	100 nF	220 nF	220 nF
	500 Hz	4.85 kΩ	4.14 kΩ	14.5 kΩ	2.04 kΩ	100 nF	100 nF	100 nF	68 nF
	1 kHz	2.43 kΩ	2.07 kΩ	16.2 kΩ	1.40 kΩ	100 nF	100 nF	100 nF	22 nF

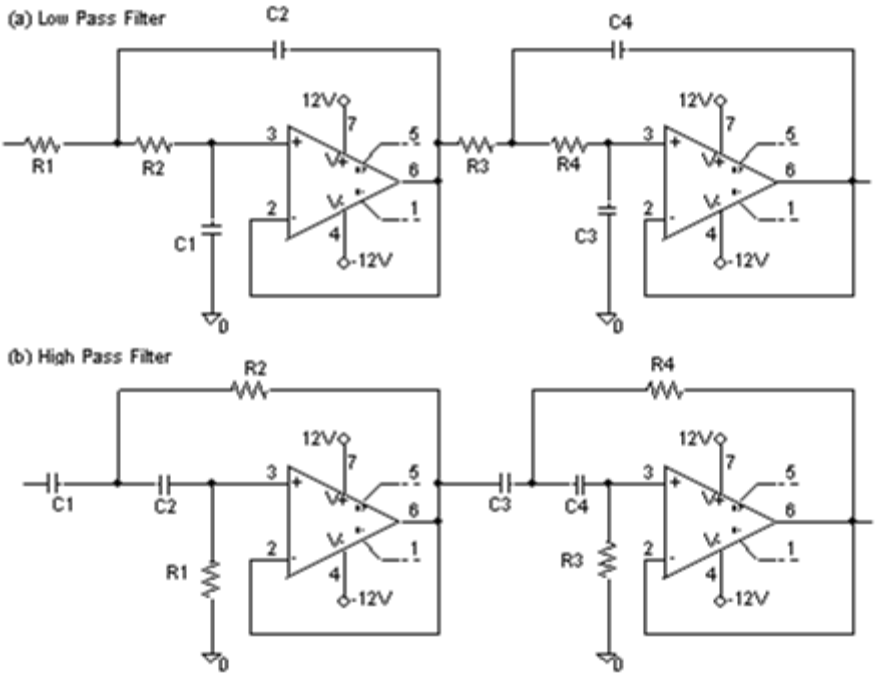

Fig. 4: Four pole Sallen-Key low-pass and high-pass filters

Figures 5 and 6 illustrate the filter selection circuitry. Because the input to the high-pass filters is linked directly to the impedance control circuit, this is the optimum place to remove any DC offset, which may be present in the input. For this reason a low voltage DC offset adjustment was added to the non-inverting terminal of the summing amplifier (Fig. 6). This circuit allows any small op-amp bias voltages to be removed from the output of the summing amplifier before proceeding to the gain control, and possibly corrupting the output. The low-pass filter selection circuitry is nearly identical to that of the high-pass block. The only

difference is that the DC offset control is not present because any significant offsets will have been removed in the high-pass stage. The switches used to operate the selection circuitry are of the double pole single throw slide type. The center tap of the switch is connected to the input of a classic summing amplifier, which is shown in Fig. 6. The other two terminals are connected to the outputs of their respective filters and to ground. The ground, or off position, assures that none of the inputs to the summing amplifier are left floating.

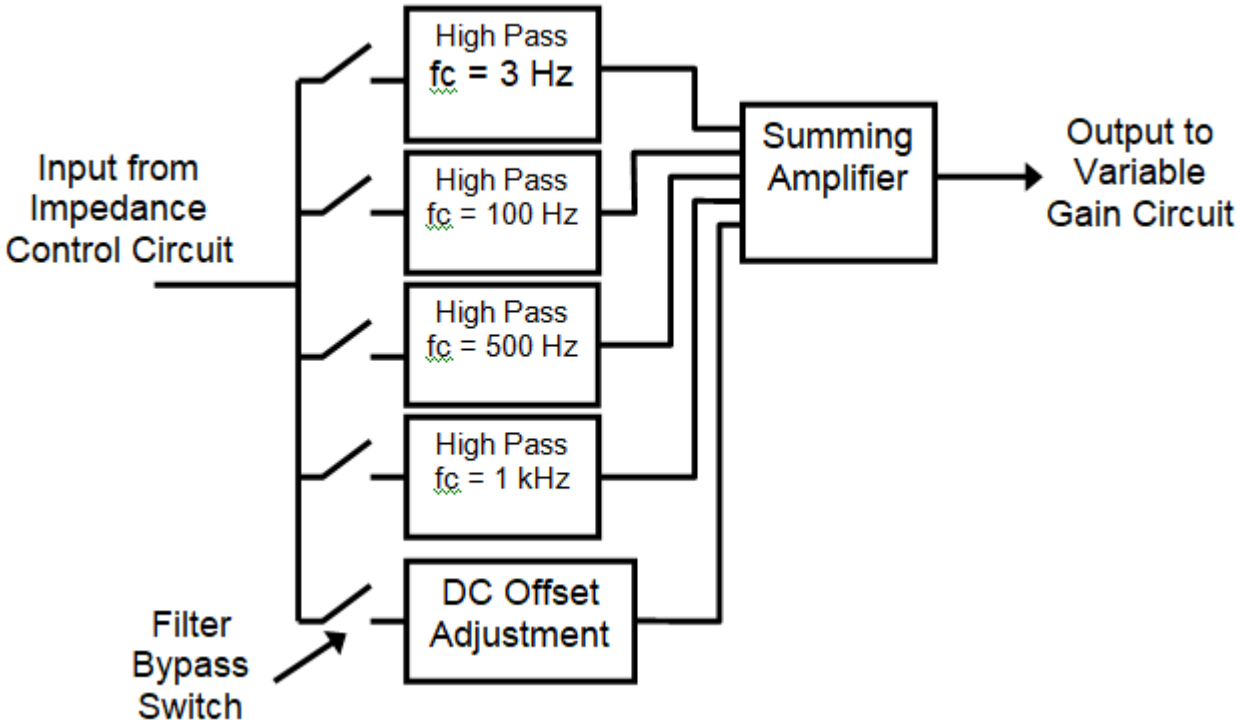

Fig. 5: High-level filter layout. High-pass and low-pass have similar configurations

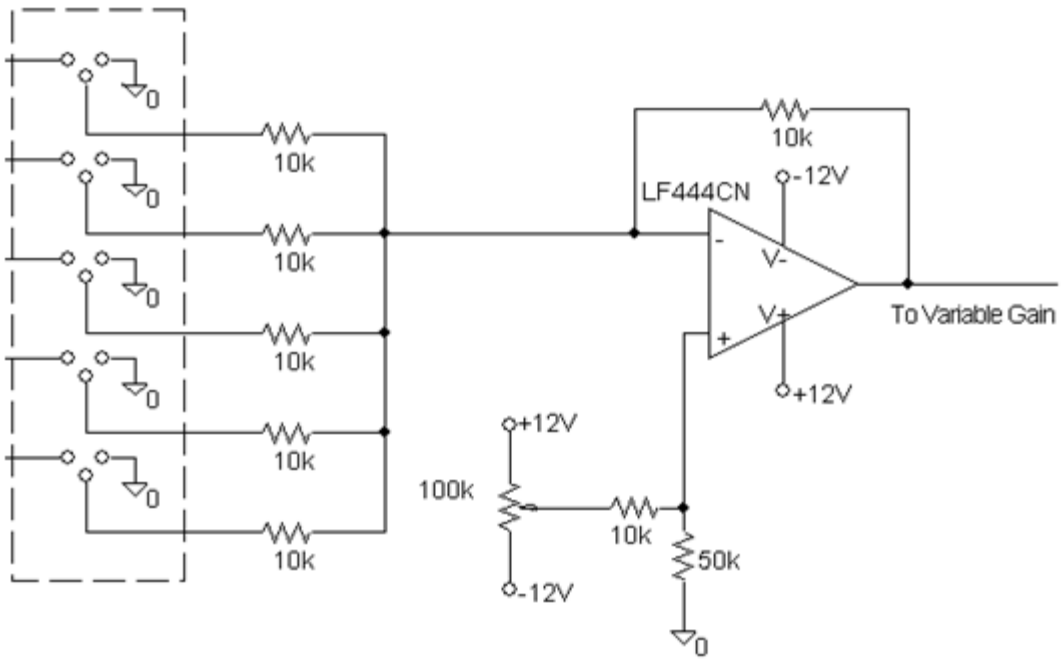

Fig. 6: Summing amplifier with filter selection

d) Amplifiers

The amplification circuit is composed of a simple inverting op-amp. Several other circuits were considered, but the inverting op-amp was selected for its ease of implementation, small number of components, and input/output impedance

characteristics. For added versatility, the gain of the inverting op-amp is controlled by shorting a series of resistors in the feedback loop of the amplifier. By connecting the resistors in series, a wide range of gains can be selected. As illustrated in Fig. 7 this circuit employs 10 kΩ, 50 kΩ, 100 kΩ, 500 kΩ, and 1 MΩ resistances allowing for gains ranging from 1X to 166X. The gain is controlled via switches that short various resistors. For example, shorting the 500 kΩ and 1 MΩ resistors yields a gain of 1X+5X+10X for a total of 16X.

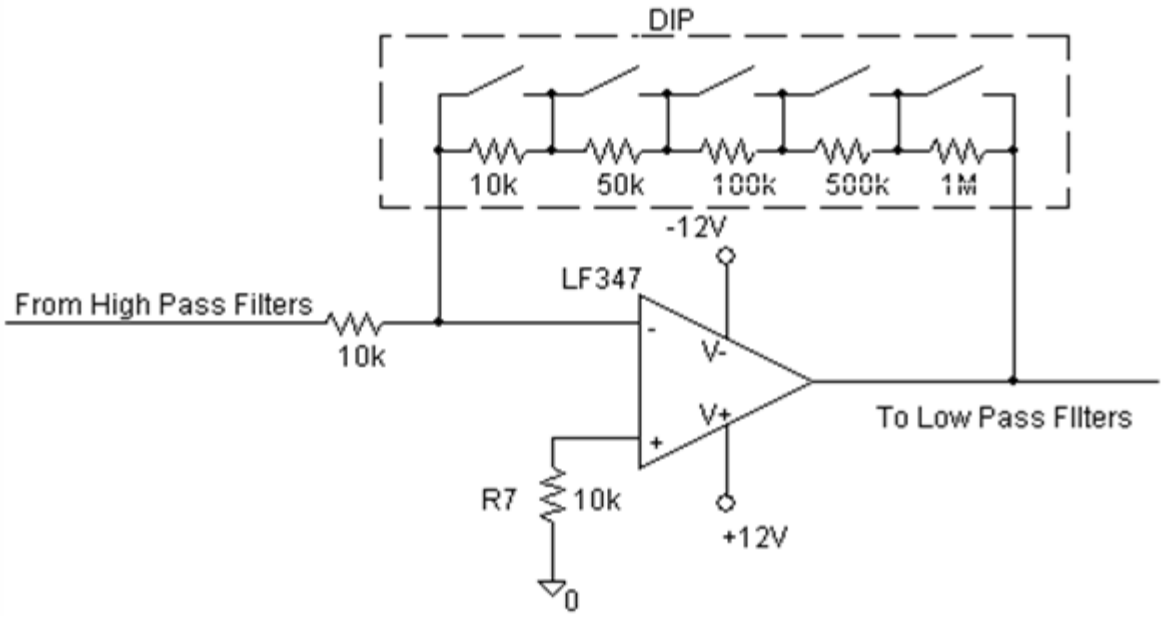

Fig. 7: Amplifier variable gain circuit. Note: The LF347 op-amp was used for testing purposes

e) Output

A visual display was added to the amplifier to alert the user of the presence of excessive g-forces. This simple readout eliminates the need to use an oscilloscope to view the output when portability is an issue. The method chosen to accomplish this task was the illumination of three LEDs. Yellow, green and red LEDs illuminate when the output of the amplifier reaches a peak value of one, seven, and ten volts respectively. Two sets of LEDs were used to indicate positive and negative g-forces. The circuit is illustrated in Fig. 8. The input is isolated by using an op-amp buffer to assure that the rectifier circuit does not interfere or load the output. It should be noted that the output of the rectifier circuit is not exactly equal to the peak AC value of the input due to the approximate 0.6V drop over the diode. This drop must be accounted for when designing the comparator circuit that lights the LEDs. The visual display circuits compare the DC voltage from the rectifier circuits with a predetermined threshold voltage. Operational amplifiers were employed here as well for design simplicity and to reduce component count.

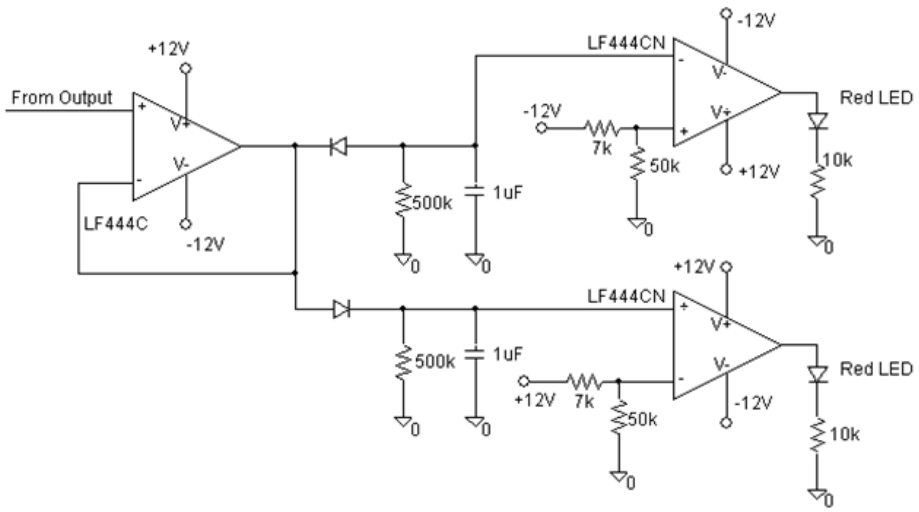

Fig. 8: Comparator and display circuit for one LED pair

The resistor values shown in this instance will cause the red LED to light at approximately 10V. One can calculate the resistor values using a voltage divider equation, remembering to add 0.6 V to the desired threshold voltage.

III. Results

Multiple mechanical frequencies must be utilized to test the accuracy of the filters and the sensitivity of the amplifier. To achieve clean consistent vibration signals, an aluminum cantilever beam was used to create vibrations and accelerations of varying amplitude and frequency (see Fig. 9). Testing of low frequencies was accomplished using the cantilever beam, while high-frequency testing was completed using an electrodynamic shaker.

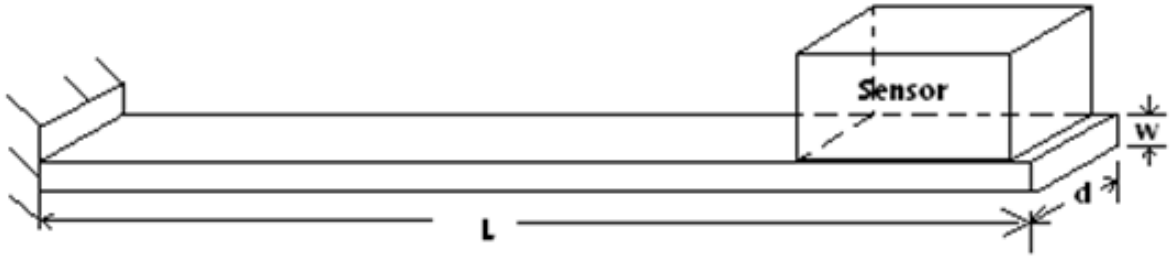

Fig. 9: The cantilever beam setup for low frequency testing

To analyze the functionality of the amplifier in a time-efficient manner, the output of the sensors was read through a data acquisition system for comparative purposes. This test arrangement was composed of the amplifier, a Keithley data acquisition board, and a computer running National Instruments' Lab VIEW software.

As with most signal amplifiers, linearity is a significant factor in this design, therefore two tests were employed to verify the efficacy of each stage. Initially, the amplifier was set to 1X gain with all filters bypassed. The input voltage was incrementally increased from 0V to 10V while recording the outputs and calculating the respective correlation coefficients. The test was repeated with one high-pass and one low-pass filter activated to validate the filter circuits. The process was then repeated for numerous combinations being careful not to saturate each stage. The worst-case deviation from linearity is illustrated in Fig. 10. With a 1X gain selected, the upper 3dB point of the amplifier is 220 kHz. With the gain set at 166X, the 3dB point is shifted to 18 kHz, reducing the operating bandwidth as expected, but still remaining within the design limits. The 3dB point for each filter was within 5% of the calculated value, and the roll-off rates exceeded 65 dB/decade.

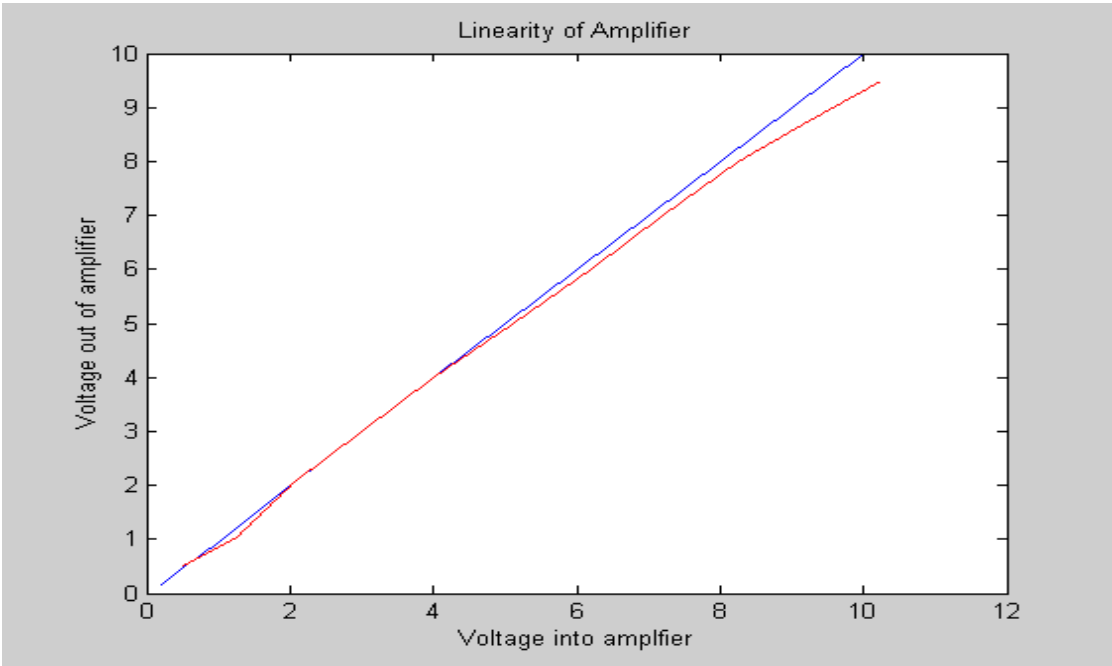

Fig. 10: Linearity test for amplifier with correlation coefficients shown

In order to scale the output correctly the gain values must be accurately known, otherwise significant errors will result when calculating the acceleration or vibration magnitudes. All five gain switches were toggled to determine the influence of each. The results are summarized in table 3. Small deviations from the predicted values can be attributed to component variations but are still within design limits. All goals of table 1 were accomplished or exceeded.

Table 3: Actual verses predicted gains

Vin	Vout	Gain	Actual Gain	%error
1.525	1.55	1	1.016	3.25%
0.31	1.575	5	5.081	1.59%
0.135	1.375	10	10.18	1.82%
0.105	5.2	50	49.52	-0.96%
0.0525	5.1	100	97.14	-2.94%
0.052	8.625	166	165.8	-0.08%

Table 4: Measured signal conditioner performance

Parameter	Measured Results
Frequency Range	0 Hz to 10 kHz, at selectable ranges
Filter roll-off	>65 dB/decade
THD	<0.012%
Linearity	0.11% deviation
Resolution	$0.04\,\mu g/\sqrt{Hz}$ in conjunction with sensor
Gain	Selectable up to 166
Thermal Stability	Minimal effect
Dynamic Range	$>50\,g$
Transverse Sensitivity	< 1%
Output	+/- 10V

IV. Conclusion

An alternative technique for analyzing signals from PVDF sensors has been introduced and this signal conditioning system has proven to be useful, inexpensive, and relatively easy to fabricate. It also provides reliable and repeatable results for several PVDF sensor models. With the output connected to an analog-to-digital converter card the signal processor described here exceeded the capabilities of similar products tested. This conditioner adds several useful features to comparable products such as a selectable gain, high-pass and low-pass filters, and a simple output indicator. This amplifier is an excellent alternative to comparable designs but at a significantly reduced cost. Its versatility makes it suitable for use with most PVDF sensors. This work was initiated from an industrial need for a simple and reliable acceleration and vibration signal conditioning system for automated integrated circuit placement, still there can be many other uses, e.g., impact sensors, flow meters, contact microphones, etc. Several sensors can be connected to similar conditioners, and by simultaneously monitoring the outputs of two or more devices, one can gain a better understanding of where vibrations are originating.

References Références Referencias

1. Measurement Specialties, Inc. Piezo Film Sensors Technical Manual. Valley Forge, PA: 1998.
2. M.F. Barsky, D.K. Lindner, R.O. Claus "Robot gripper control system using PVDF piezoelectric sensors," *IEEE Transactions on Ultrasonics, Ferroelectrics, and Frequency Control,* vol. 36, no.1, pp.129-134.
3. W. Galbraith, G. Hayward, "Development of a PVDF membrane hydrophone for use in air-coupled ultrasonic transducer calibration," *IEEE Transactions on Ultrasonics, Ferroelectrics, and Frequency Control,* vol. 45, no.6, pp.1549-1588.
4. Kimoto, Sugitani, Fujisaki, "A multifunctional Tactile Sensor Based on PVDF Films for Identification of Materials. IEEE Sensors Journal, Vol 10, Issue 9.
5. F. Bauer, "PVDF shock sensors: applications to polar materials and high explosives," IEEE *Transactions on Ultrasonics, Ferroelectrics and Frequency Control,* vol 47, no. 6, pp. 1448-1454.
6. J.M. Gonnet, J. Guillet, G. Boiteux, R. Fulchiron, G. Seytre, "Dielectric studies of PVDF crystallization. Application to in-situ monitoring in injection

molding," IEEE *Transactions on Dielectrics and Electrical Insulation,* vol 8, no. 6, pp. 911-916.
7. A. Selfridge, P.A. Lewin, "Wideband spherically focused PVDF acoustic sources for calibration of ultrasound hydrophone probes," IEEE *Transactions on Ultrasonics, Ferroelectrics and Frequency Control,* vol 47, no. 6, pp. 1372-1376.
8. F. Bauer, "PVDF Shock Sensors: applications to polar materials and high explosives. IEEE Transactions on Ultrasonics, Ferroelectronics, and Frequency Control. November 2000.
9. Hutchinson, Michael. Design of self Calibrating Piezoelectric Polymer Based Accelerometer. State College, PA: Penn State University. 1996.
10. S. Rajala, J. Lekkala,, Film-Type Sensor Materials PVDF and EMFI in Measurement of Cardiorespiratory Systems – A Review. IEEE Sensors Journal, Vol. 12, Issue 3.
11. Y. Ting, C. Chang, H. Gunawan, "Circuitry Design for Direct Wind Energy Harvest System" 2010 IEEE International Symposium on Industrial Electronics.
12. Hill, Winfield., and Paul Horwitz. Art of Electronics. 2nd ed. New York, Cambridge University Press, 1989.
13. Dorf, Richard C. The Electrical Engineering Handbook. Ann Arbor, MI: CRC Press, 1993.
14. Sedra and Smith Microelectronic Circuits 7th ed. New York. McGraw Hill. 2015.